Editors' Suggestion

Structure analysis of PTCDA/Ag(100) by low-energy electron diffraction and density functional theory

Ina Krieger and Moritz Sokolowski*
Clausius-Institut für Physikalische und Theoretische Chemie, Universität Bonn, 53115 Bonn, Germany

Anja Haags
Clausius-Institut für Physikalische und Theoretische Chemie, Universität Bonn, 53115 Bonn, Germany and Peter Grünberg Institut (PGI-3), Forschungszentrum Jülich, 52425 Jülich, Germany

Thomas Bredow
Mulliken Center for Theoretical Chemistry, Clausius-Institut für Physikalische und Theoretische Chemie, Universität Bonn, 53115 Bonn, Germany

Christian Kumpf and F. Stefan Tautz
Peter Grünberg Institut (PGI-3), Forschungszentrum Jülich, 52425 Jülich, Germany; Jülich Aachen Research Alliance (JARA), Fundamentals of Future Information Technology, 52425 Jülich, Germany; and Experimentalphysik IV A, RWTH Aachen University, 52074 Aachen, Germany

Georg Held
Diamond Light Source Ltd, Oxfordshire OX11 0DE, United Kingdom

(Received 12 June 2025; revised 21 November 2025; accepted 24 November 2025; published 23 February 2026)

The adsorption geometry of the planar 3, 4, 9, 10-perylene-tetracarboxylic-dianhydride (PTCDA) molecule in the commensurate c(8 × 8) structure on Ag(100) was determined from the analysis of the intensities in low-energy electron diffraction (LEED-IV). Using data from different angles of incidence and optimized computer code, we were able to overcome earlier challenges given by the limitations of the experimental data set and the calculation times required for the large unit cell with many atoms. Testing of different structures confirmed the on-top adsorption site for the center of the perylene core. The final Pendry R factor of $R_P = 0.180$ for the on-top position is significantly lower than the one for the fourfold hollow position (minimum $R_P = 0.369$) that is hence excluded. The molecule shows archlike deformation with a downshift of the terminal carboxylic groups. Both the molecular structure and the adsorption height are in very good agreement with results from an earlier normal incidence x-ray standing wave (NIXSW) experiment and new density functional theory (DFT) calculations, which we performed in parallel for 0 K and in addition for 300 K. The LEED-IV analysis demonstrates that the PTCDA induces a relaxation (−0.08 versus −0.04 Å of the clean surface) and buckling (0.33 Å) of the topmost Ag layer. Special attention was given to the Ag atom below the central ring of the PTCDA. The IV analysis was rather insensitive to its vertical position, and a small R factor, close to the minimal, was also obtained when this Ag atom was moved upward ($R_P = 0.185$) or even an Ag vacancy site ($R_P = 0.171$) was assumed. However, these structures could be excluded on the basis of DFT calculations. The vacancy structure has a free adsorption energy that is 0.18 eV larger compared to the favored geometry where this central Ag atom is pushed downward, partly due to the energy cost for the vacancy formation. The discussion of adsorbate-induced formation of vacancy sites is important because it was reported for C_{60} on Ag(111). The up- and downward displacements of the first-layer Ag atoms support the understanding of the chemical bond of the PTCDA to the Ag substrate and reveal how the originally planar π system is locally distorted. Our analysis proves that LEED-IV is a powerful technique for surface crystallography of large organic adsorbates.

DOI: 10.1103/gxh1-b3w4

I. INTRODUCTION

Over the last years, the understanding of the adsorption of larger π-conjugated molecules on surfaces has been in the focus of interest. Hereby, one of the key questions concerns the modifications in the geometric and electronic structures of the molecules and the substrates, induced by the chemical bonds that are established across the interface [1]. Evidently, quantitative information on the positions of all involved atoms, those of the adsorbate and of the substrate, is most desirable here, and constitutes the basis for interpretations. Our following introduction to this topic is comprised of two parts. First, we resume the

*Contact author: sokolowski@uni-bonn.de

role of low-energy electron diffraction (LEED) for structural investigations of organic molecules. In the second part, we introduce the specific 3,4,9,10-perylene-tetracarboxylic -dianhydride (PTCDA)/Ag(100) system, which is subject of this work.

A. Structural analysis of larger organic adsorbates by low-energy electron diffraction

There are several experimental techniques that, in principle, can provide the required structural information [2]. Among these, dynamical low-energy electron diffraction (LEED-IV), is the most established one. LEED-IV has been successfully used to unravel a large number of structures of bare surfaces and surfaces on which atoms or small molecules were adsorbed [3]. Some smaller organic molecules have also been studied, e.g., glycine, formic acid, and benzene [4–6]. However, in view of larger organic molecules, e.g., those comprising several benzene rings, LEED-IV has been used only very sparsely so far [7]. This is at least partly related to several systematic challenges, which we will address further below.

A more recent technique that has now been widely applied for the structure determination of larger, in particular flat-lying π-conjugated molecules on surfaces, is the normal incidence x-ray standing waves (NIXSW) method [8]. In an NIXSW experiment, the relevant signal is given by the photoemission yield of a specific atomic species of interest. As long as the photoemission signals of different species can be discerned, NIXSW can be used to determine their individual positions. However, this is generally not possible for atoms of the substrate, and for atoms in the molecule of the same element that are chemically too similar to be distinguished by their spectral signature in photoemission. In that situation, only averaged information is retrievable. As a consequence, some interesting aspects of the adsorption geometry are inaccessible by NIXSW, such as, e.g., the substrate relaxation and reconstruction, and the coordinates of chemically similar adsorbate atoms that are not distinguishable in photoemission, e.g., the C atoms located in the cores of π-conjugated molecules. This information can be gained from a LEED-IV analysis, as we will show.

In short, the first step of a LEED-IV analysis requires recording the integrated intensities of the LEED spots as a function of electron energy (IV curves). Figure 1 displays such an LEED image with distinct spots. In a second step, theoretical IV curves are calculated for a hypothetical structure and compared to the experimental ones. The coordinates of the model are optimized until the best agreement of the experimental and theoretical curves is obtained [3]. In general, the analysis requires that the summed-up energy range ΔE_{total} of the IV curves, which were measured on symmetry nonequivalent LEED spots, exceeds a certain value that is proportional to the number of determined structural coordinates (typically $\sim$50 eV per coordinate).

As larger organic adsorbates exhibit larger unit cells compared to small ones, the superstructure spots are closer together in the LEED image. This makes it experimentally more difficult or even impossible to determine their individual intensities from the recorded LEED images, in particular, at higher energies when the k space is compressed on the LEED screen (typically above 120 eV). This limits the energy range of the data and hence its information content. As we will report, it can be compensated to some extent by measuring the IV curves at different angles of incidence of the primary electron beam with respect to the sample surface, since this lifts the equivalency of those spots which are symmetrically equivalent at normal incidence. This approach is not used in standard LEED-IV experiments, where normal incidence is preferred in order to exploit the underlying symmetry in the calculations. However, when this aspect is sacrificed, IV curves taken at different angles of incidence can help to extend the data range, leading to a higher reliability of the analysis [9,10].

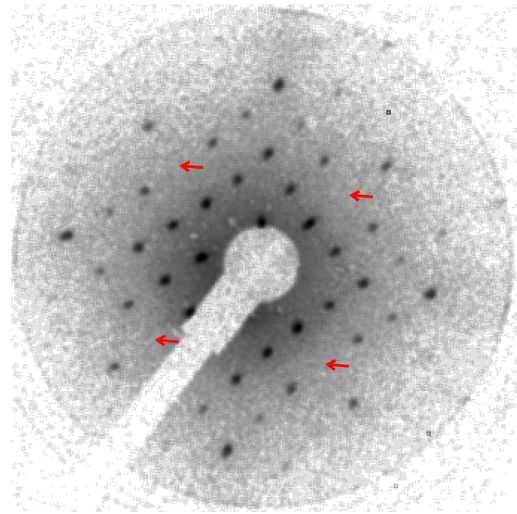

FIG. 1. LEED pattern of the commensurate monolayer structure of PTCDA on Ag(100). The pattern was recorded using an MCP-LEED optics at an electron energy of 39 eV and a sample temperature of 120 K. The (0,0) spot is hidden behind the electron gun located in the center of the pattern. The higher-order spots are subject to a cushion distortion due to the flat screen of the MCP-LEED optics. Notably, only one domain exists for this superstructure. The red arrows mark the positions of the missing spots due to the glide-plane symmetry.

A second aspect that has a similar impact on the data acquisition is given by a possible electron-induced beam damage of organic adsorbates and weak spot intensities. This latter aspect can partly be addressed by using a micro channel plate (MCP) LEED apparatus, which provides an increased sensitivity with respect to a conventional LEED apparatus. Therefore, such LEED instruments can be operated with primary currents in the 1 nA range, which amounts to about 10^{-3} electrons per second and surface atom, enabling the collection of sufficient data with minimum beam damage. Finally, the LEED-IV calculations of larger organic adsorbates suffer from computer time limitations. Due to the large number of atoms within the unit cell and the respective large number of coordinates that have to be optimized, the calculations become very time-consuming, and an effective structure search is prohibited. Today, this limitation is resolved to some extent by faster computers. In addition, we benefited from the high efficiency of the specific computer code for the calculation of the

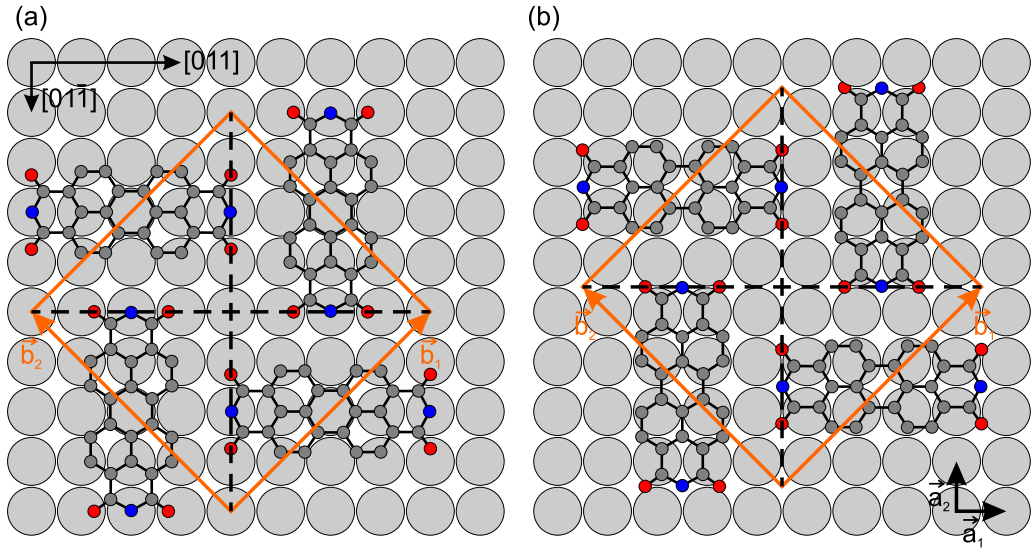

FIG. 2. Models of the possible superstructures of PTCDA on the Ag(100) surface. The molecules exhibit a T-shape arrangement with a fourfold rotational axis. In (a), the adsorption site is the fourfold on-top site, in (b), it is the fourfold hollow site. The fourfold on-top site is the correct site and was verified by NIXSW [1]. The PTCDA molecules are shown as ball-and-stick models. The hydrogen atoms are omitted. Carboxylic O atoms are red, anhydride O atoms are blue, and the carboxylic C atoms and those of the perylene core are gray. The unit cell, given by the vectors ($\mathbf{b}_1$, $\mathbf{b}_2$), is marked by the orange lines. The substrate vectors ($\mathbf{a}_1$, $\mathbf{a}_2$) are also indicated. The two glide lines of the structure are marked as dashed lines.

theoretical IV curves that was developed by one of the authors (G.H.) [11].

B. Introduction to PTCDA/Ag(100)

Here, we report a LEED-IV analysis on the prototypical molecule PTCDA adsorbed on the Ag(100) surface [1,12]. The structure of the PTCDA molecule is shown in Figs. 2 and 4(a) (below). It consists of a perylene core that is terminated by two anhydride groups on opposite sides. The groups have proven to be relevant for the bonding of the molecule to the substrate [1]. The scope of the present work is twofold. First, we showcase how the LEED-IV technique can be used successfully for the analysis of the structure of a larger π-conjugated molecule. Secondly, we report interesting new aspects that we have found by this analysis for PTCDA adsorbed on the Ag(100) surface, but which are presumably of a more general nature and will thus apply to similar systems, too. These aspects concern, in particular, the vertical distortion of the perylene backbone and the reconstruction, i.e., the buckling of the underlying Ag substrate.

PTCDA/Ag(100) lends itself to the purpose of a LEED-IV feasibility study for several reasons. First of all, it forms a highly ordered commensurate superstructure of high symmetry. Different from many other similar molecule/substrate combinations, there exists only the domain shown in Fig. 2, but no other rotation/mirror domains. This aspect implies that the number of independent structural coordinates that have to be determined is not too large, and the structure search by LEED-IV simulations is hence not too time-consuming. An exemplary LEED image is given in Fig. 1. Secondly, PTCDA/Ag(100) was investigated by NIXSW before, and the vertical heights of chemically discernible atoms have been determined [1]. A comparison of the results of both techniques (NIXSW/LEED-IV) is thus possible and can highlight their specific strengths and weaknesses. Moreover, density functional theory (DFT) results were also available [1] and were amended by novel and advanced nonzero temperature DFT calculations within the scope of the present work. Besides what has been said for NIXSW already, the DFT results can guide the LEED-IV analysis for structural parameters that are inaccessible by NIXSW, e.g., the substrate reconstruction. Last, but not least, it was found by DFT and NIXSW that the intrinsically planar PTCDA molecule distorts into an archlike configuration upon adsorption on the Ag(100) surface, where the terminal oxygen atoms are located closer to the substrate than the central perylene core. DFT also revealed a concomitant buckling of the first Ag layer by 0.19 Å. [1]. Because of all of these results, PTCDA/Ag(100) constitutes an interesting case study for LEED-IV.

Before we turn to the details of our LEED experiment, we recapitulate some properties of the superstructure of PTCDA on the Ag(100) surface. The commensurate superstructure exhibits a square unit cell and belongs to the space group *p4gm* [12]. The structure is illustrated in Fig. 2. The panels (a) and (b) show the situations for the two fourfold adsorption sites (fourfold on-top and fourfold hollow) that are compatible with the symmetry of the unit cell. The on-top site is the correct site (see below). The superstructure was also confirmed by scanning tunneling microscopy [12]. The unit cell is given by the vectors ($\mathbf{b}_1$, $\mathbf{b}_2$) and is $p(4\sqrt{2}\times 4\sqrt{2})\mathrm{R}\,45^\circ$ in Wood notation. Alternatively, it can be described by the matrix

$$\begin{pmatrix}\mathbf{b}_1\\ \mathbf{b}_2\end{pmatrix} = \begin{pmatrix}4 & 4\\ -4 & 4\end{pmatrix}\begin{pmatrix}\mathbf{a}_1\\ \mathbf{a}_2\end{pmatrix}, \tag{1}$$

where $\mathbf{a}_1$ and $\mathbf{a}_2$ denote the vectors of the substrate. The unit cell contains two PTCDA molecules in planar adsorption

geometry, orientated perpendicular to each other, yielding a T-shape arrangement [12]. The structure can also be labeled $c(8 \times 8)$ (with a unit cell containing 4 molecules) [12]. This is sometimes useful, as the larger unit cell shows the symmetry elements more clearly. This larger unit cell is shown in Appendix A.

The space group *p4gm* exhibits two glide lines, which are indicated as dashed lines in the horizontal and vertical directions in Fig. 2. They lead to systematic extinctions in the LEED pattern (Fig. 1) of the $(0, \frac{2n+1}{4})$ and $(\frac{2n+1}{4}, 0)$ spots, n being an integer number. In Fig. 1, this is seen for the spots in the directions of $\sim \pm 45^\circ$ with respect to the horizontal direction indicated by the red arrows.

As mentioned above, only two adsorption sites are compatible with the symmetry of the superstructure, namely the fourfold on-top site and the fourfold hollow site. Both sites are shown in Fig. 2 in panels (a) and (b). All other adsorption sites, e.g., a bridge-site, can be excluded, as they are incompatible with the *p4gm* space group. The on-top site was experimentally verified by us within an NIXSW experiment [1]. For this purpose, we performed a triangulation [13], similar to that reported for PTCDA/Cu(100) [14].

Furthermore, a LEED-IV experiment of the clean Ag(100) surface was executed to test possible relaxation of the Ag layers and to compare it to previous literature results, which predict no relaxation of the substrate [15]. They are reported in Appendix B. These results can be used to compare the structural changes for the relaxation of the Ag layers after adsorption of PTCDA.

II. EXPERIMENTAL DETAILS

The experiments were carried out under ultrahigh vacuum (UHV) conditions in a UHV chamber at a base pressure of 4×10^{-10} mbar. The chamber was μ metal shielded and equipped with a three-grid microchannelplate (MCP)-LEED optics manufactured by OCI Vacuum Microengineering (Canada). The MCP allows to use low emission currents in the nA range [16]. This is advantageous to keep the radiation damage of the organic adsorbate by the electrons at a minimum. The Ag(100) single crystal was mounted onto a manipulator and prepared by repeated cycles of Ar sputtering, followed by annealing at 950 K, until the surface showed a high structural quality as controlled by LEED. PTCDA was evaporated from a well-outgassed home-built Knudsen cell at a temperature of ~640 K with a rate of 0.4 monolayer/min. The purity of the PTCDA beam and the deposition rate were monitored by a quadrupole mass spectrometer [17]. The sample was held at room temperature (~300 K) during the deposition of the PTCDA layer. For optimization of the lateral order and to desorb unwanted second-layer molecules, a mild annealing cycle at 420 K for 10 min was used. For the subsequent LEED experiments, the sample was cooled to about 120 K by liquid nitrogen in order to keep the thermal background small.

We performed all MCP-LEED measurements using energy steps of 1 eV with an energy range from 50 to 300 eV for the clean Ag(100) surface, and from 18 to 350 eV for PTCDA on Ag(100). The maximum duration of the measurements was 20 min per sample position, starting at low energies. In order to minimize electron-induced damage, the sample current was kept in the 1 nA range. For a beam diameter of 0.5 mm, this corresponds to a dose of about 50 electrons per PTCDA molecule. It was carefully checked that the maximum of intensity of the (1,1) spots at 100 eV did not decrease by more than 10% within 30 min of electron irradiation. The LEED patterns were recorded as a function of energy using a video-based and computer-controlled measuring system with a 10-bit CCD camera. Figure 1 shows an exemplary LEED pattern. The beam current, the voltage applied to the MCP plate, and the exposure time of the CCD camera were carefully adjusted to safeguard that the intensities of the relevant LEED spots did not saturate. A nonlinear scaling of the intensities by the MCP is possible, but was acceptable, as the R factor mainly depends on the modulation of the intensities as a function of energy.

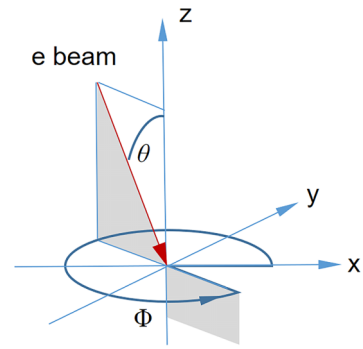

FIG. 3. Geometry of the LEED experiment defining the angles of incidence θ and Φ. θ is the angle of the incident beam with respect to the surface normal and Φ is the angle between the crystal x axis and the projection of the incident beam on the crystal surface.

The polar angle θ is the angle of the incident beam with respect to the surface normal and was adjusted in a range of $\pm 10^\circ$. The azimuthal angle Φ is the angle between the crystal x axis (direction of $\mathbf{a}_1$ in Fig. 2) and the projection of the incident electron beam onto the crystal surface. It could not be varied due to the experimental setup of the sample holder/manipulator. In Fig. 3, this geometry of the experiment is illustrated. The experimentally set values of θ and Φ are subject to some uncertainties related to the sample manipulator. Hence, their values were also considered as free parameters in the LEED-IV structure search.

With the experimental setting, 17 integer order spots were visible in the energy range from 18 eV to 350 eV; while 52 fractional order spots could be recorded between 18 and 120 eV. Experimental IV curves were extracted using the Igor data analysis environment and a routine written by one of the authors (G.H.). The IV curves were obtained for five different polar angles, θ, nominally 0°, $\pm 5^\circ$, and $\pm 10^\circ$. In order to save computer time and to perform the structure optimization within a reasonable time, only data for 0, $+5^\circ$, and $+10^\circ$ were used for the structure optimization. In the preparation of these experiments, we also performed a LEED-IV analysis of the clean Ag(100) surface. This is described in Appendix B.

III. LEED-IV CALCULATIONS AND STRUCTURE OPTIMIZATION

The data analysis was performed with the fully automated CLEED program package [11], which is able to determine the surface geometry using LEED-IV data taken at different angles of incidence simultaneously. In total, data of three polar angles, around 0°, 5°, and 10°, were included. CLEED uses fully dynamical scattering theory along the lines of algorithms developed by Pendry [18] and Van Hove & Tong [19]. Bulk scattering was calculated using Pendry's layer doubling method with vertical bulk inter-layer distances of 2.04 Å for Ag{100}. Convergence is typically achieved by including 16 bulk layers. The scattering phase shifts representing the scattering factors of individual atoms within the structure were calculated as a function of energy using the program package provided by Barbieri and Van Hove [20]. LEED-IV calculations were performed in the energy range 20 to 150 eV. The relatively low electron energies allowed to limit the maximum angular momentum quantum number $l_{\max}$ to 6 without compromising the accuracy of the calculation. The imaginary and real parts of the crystal potential were set to −4.0 and −8.0 eV, respectively. The radial root mean square (*rms*) displacements of the Ag atoms, which describe their thermal vibrations, were optimized to 0.03 and 0.05 Å for bulk and surface atoms, respectively, using the LEED-IV data for the clean surface. For the oxygen and carbon atoms, constant *rms* displacement values of 0.05 Å were used in accordance with earlier work [4]. Hydrogen atoms were ignored in the LEED calculations as it is common practice because of their small scattering cross section, which has only an insignificant impact on the positions determined for the heavier atoms [21].

The downhill simplex method was used for optimizing the structural parameters and the exact angles of incidence [22]. The latter is necessary because the accuracy of manipulator readings and sample alignment in the experiment was less than the sensitivity of the IV curves to changes in the angle of typically ≈0.1°. As the LEED pattern near normal incidence (Fig. 1) clearly shows missing $(0, \frac{2n+1}{4})$ and $(\frac{2n+1}{4}, 0)$ spots, indicating a glide line along the [011] and [0$\bar{1}$1] directions (see Fig. 2), the structure optimization was constrained such that the glide-lines and fourfold rotation symmetry are maintained for the adsorbate and the underlying Ag layers. As a result, only one rotational/mirror domain of PTCDA/Ag(100) had to be considered.

Each PTCDA molecule contains 24 carbon atoms, 6 oxygen atoms, and 8 hydrogen atoms, the latter of which were omitted in the calculation and structure optimization. In addition, the atomic positions of the first and second Ag layers were optimized, each of which contains 32 atoms within the primitive unit cell. Therefore a total of 124 atoms (60 atoms for two PTCDA molecules per unit cell plus 64 Ag atoms) were included in the optimization.

Throughout the structure optimization, the atomic coordinates of the molecules and underlying Ag layers were constrained such that a local C_{2v} symmetry was maintained for the adsorption complex within the overall $p4gm$ space group symmetry with a fourfold rotation axis and two glide-lines. As a consequence, all C and O atoms can be described by 7 and 2 symmetry-independent atoms, respectively. Likewise, the first and second Ag layers can be reduced to 7 and 4 independent atoms, respectively. Atoms which are not symmetry-equivalent are indicated by different colors and numbers for each layer in Figs. 4(a)–4(c). If not specified otherwise, the vertical coordinates of all independent atoms were optimized; in addition, two parameters (α_l and α_s) were included, representing a uniform and symmetric stretch of the molecules along the two local mirror planes of the molecule along its long and short axes [see Fig. 4(a)]. This leads to a total of $9 + 7 + 4 + 2 = 22$ structural parameters plus $3 \times 2 = 6$ parameters related to the two angles of incidence (θ and Φ) for each of the three data sets to be optimized. Typical computing times amounted to 20 min per iteration.

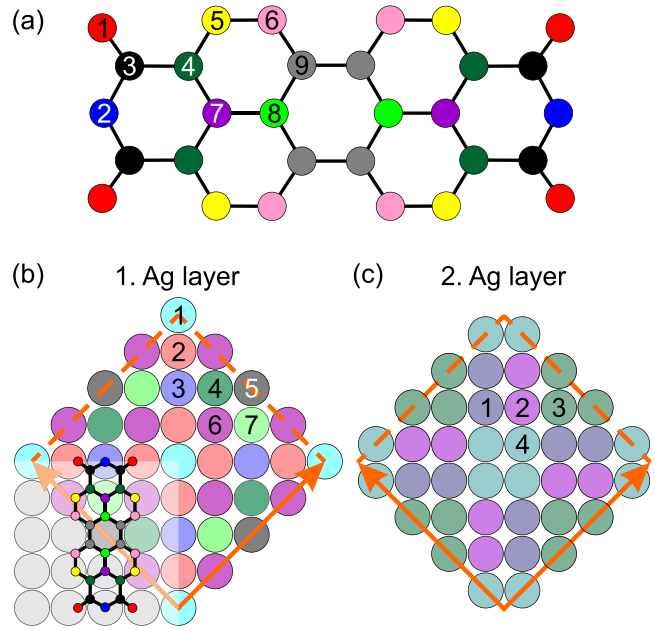

FIG. 4. (a) Ball-and-stick model of PTCDA. H atoms are omitted, O_{carb}/O_{anhyd} (1,2) are in red/blue color, and the 7 chemically different C atoms (3 to 9) are marked by different colors and numbers. Due to the fourfold symmetry of the adsorption site, these 9 different atoms remain valid for the adsorbed molecule, as indicated in (b). (b) and (c) show hardsphere models of the first and the second Ag layer with the unit cell indicated by red arrows and dashed lines. Ag atoms, which are on symmetry inequivalent sites, are again marked by different colors and numbers. In (b), only one of the two PTCDA molecules per cell is shown for the sake of clarity.

We note that we alternatively tried to describe the molecular distortion by a set of Fourier components related to the in-plane waves of the superstructure. Such an approach was used in Ref. [23]. It effectively couples the distortions of atoms that are laterally closer to each other. However, this approach turned out as a dead end here, since the *R* factor optimization did not find the same, but only less deep, minima compared to the search with discrete vertical coordinates. We suppose that this is due to the different type of the *R* factor hypersurface, and the fact that the vertical distortions of the PTCDA molecule appear on a

rather short-range length scale, compared to the situation in Ref. [23].

The agreement between the experimental and theoretical IV curves was quantified with Pendry's R_P factor and the error margins for the coordinates of the final structure were calculated using the *RR* factor method [24]. The cumulative energy overlap of all IV curves was around 4500 eV, which results in a *RR* factor of 8.4%. The overall R_P factor, which was used for the structure optimization, is a weighted average over all angles of incidence, whereby the relative contribution of each angle depends on the cumulative energy range of the individual angles. The optimization was considered converged once the R_P factors of all geometries within the simplex (cf. Ref. [22]) were within 0.0005. The error bar for each optimized atom coordinate was then determined by displacing the respective coordinate from the minimum position until R_P increased by $RR \times R_{P,min}$. The complete set of experimental and theoretically calculated IV curves for the best-fitted geometries is given in Ref. [25].

As noted, the angles of incidence θ and Φ were also optimized during the structure search. For the favored structure model (see below) the fitted values of θ were 0.4°, 4.4°, and 8.1°, which are in good agreement with the manipulator settings of 0.0°, 5.0°, and 10° within the mechanical inaccuracy of the sample mounting. This demonstrates the effective fitting of the incidence angle during the search.

IV. DFT CALCULATIONS

As we will report below, the LEED-IV analysis provided several minima of the *R* factor. In order to identify the correct and physically plausible structure, we hence performed additional DFT calculations. With respect to earlier calculations performed on this system [1], these utilized the recently developed meta-GGA functional r^{2}SCAN [26], which was shown to provide accurate structures and energies [27]. As in our earlier study, optimizations were performed with the plane-wave code VASP [28,29], employing the projector-augmented wave method [30,31]. However, different from the former, in our present calculations we have included thermal effects from phonons, which means that zero-point energies and thermally excited states at $T = 300$ K were included in the calculation of the internal energies U and Helmholtz free energies F. The inclusion of thermal excitations led to a significant increase in computing times, but was required here as we had to calculate small differences in energies with sufficient accuracy in order to discriminate between different adsorption models.

The following further details of the VASP calculations are important. (a) The r^{2}SCAN functional was augmented with dispersion corrections using the D3 method [32]. (b) A high kinetic energy cutoff (900 eV) was employed to define the plane-wave basis set in order to approach the basis set limit. (c) High-quality POTCAR files were employed from the potpaw_PBE.54 suite, Ag_sv_GW (05Dec2013), C_GW_new (17Jan2021), O_GW_new (16Dec2020), and H_GW (21Apr2008). (d) The numerical precision for integration was set to *Accurate*. (e) SCF tolerance was set to a small value, i.e., 1.0×10^{-7} eV. (f) Geometry optimization was performed with a preconditioned LBFGS optimizer [33] as implemented in the Atomic Simulation Environment [34]. Our tests showed that this optimizer is more efficient and provides lower-energy minimum structures compared to the built-in optimization algorithms in VASP. VASP was employed as a calculator in these optimization runs. (g) The same three-Ag-layer slab models, based on the superstructure of Eq. (1), as in our previous study, were employed to model the PTCDA/Ag(100) surface [1], applying a $3 \times 3 \times 1$ Monkhorst-Pack grid for integrations in reciprocal space. The slabs were separated from each other by 20 Å of vacuum. The Ag atoms in the bottom layer, i.e., the second layer below the surface, were kept fixed. We tested for convergence of the calculations for the three-Ag-layer slab. For example, for the surface vacancy defect (see below), where this is in particular relevant, the formation energies (excluding the energy gain due to re-adsorption of the expelled Ag atom) changed only minutely from 0.86 eV to 0.88 eV when going from three to four Ag layers. (h) The calculated Ag lattice constant with r^2SCAN-D3/900 eV was 4.068 Å and differed thus only by 0.5% from the experimental value of 4.085 Å (see below). (i) For the phonon calculations, we had to use a lower theoretical level since phonon calculations at the r^2SCAN-D3 level were computationally too demanding. These were performed with GPAW (version 24.1.0) [35] using the *CrystalThermo* utility. The force-constant matrix was calculated with PBE-D3 and a 520 eV cutoff and the Γ-point approximation. The phonon frequencies were obtained within the harmonic approximation. As in the geometry optimizations, the Ag atoms of the first layer and all atoms of the PTCDA monolayer were included in the phonon calculations. The zero-point corrections and thermal contributions of the phonons to U and F at 300 K were calculated from their frequencies by applying standard approaches from statistical thermodynamics. The computed values were added to the energies obtained from r^2SCAN-D3 and a 900 eV cutoff. The entropy related to the phonon excitations, which contributes to F, was obtained likewise. The relevant formulas are given in Appendix C.

V. RESULTS

A. Identification of the adsorption site from LEED-IV and DFT

The overall symmetry of the surface allows two lateral adsorption geometries of PTCDA with respect to the {100} surface, as depicted in Fig. 2. The center of the molecule needs to coincide with a surface site with fourfold symmetry, i.e., either on top of a Ag atom [panel (a)] or a hollow site [panel (b)].

The optimization was started with planar molecules and Ag layers. For each of the two models, the start geometry of the Ag layers was either in their bulk-terminated positions or had the first-to-second layer distance contracted by 0.2 Å (nonbulk positions), as contracted layers are often found for molecular adsorbates. The vertical height of the molecules in the start geometries was always 2.6 Å above the first Ag layer, as suggested by the earlier NIXSW and DFT results [1]. Throughout, the tabulated lattice constant of 4.085 Å for Ag at room temperature was used, which implies vertical inter-layer

distances of 2.043 Å in the bulk. The lateral coordinates of the C and O atoms of PTCDA were derived from DFT-calculated coordinates for a PTCDA molecule in the gas phase in combination with the structure model of Fig. 2(a). In particular, we have used the coordinates of PTCDA supplied by P. Puschnig [36]. Evidently, the intramolecular bonds can be slightly modified upon adsorption. However, as such lateral changes in the molecular skeleton are usually small [37], and as LEED is much less sensitive to lateral than to vertical displacements, this geometry is very reasonable for the start of the search.

Typically, the optimizations required around 1500 iterations to converge. They show a clear preference for the on-top models, with $R_P = 0.180$ and 0.185 versus 0.369 and 0.413 for the hollow-site models (here, the first numbers refer to the optimization starting from bulk-terminated Ag positions, while the second numbers belong to the optimization starting with contracted first-to-second layer distances) [38]. The hollow-site models will be dismissed henceforth as their R_P values are well outside the error range of 8.4% from the minimum R factor of 0.180. For an illustration of the experimental and calculated IV curves we refer to Fig. 5; the full set of curves is given in Ref. [25]. The two remaining on-top geometries are different from each other structurally, but both yield R factors that are well within the error bar of the minimum R_P factor.

The vertical coordinates of these two geometries are given in Table I. Both models show similar adsorption heights and similar distortions of the formerly planar PTCDA molecule, within 0.1 Å. The only significant difference is found in the vertical positions of the Ag atom number 5 (Ag5), which is located below the center of the molecule and defines the on-top site (cf. Fig. 4). When starting the optimization from bulk-terminated Ag layer positions, this atom relaxes to a vertical position 0.19 Å below the average height of the topmost Ag layer (noted as Ag5-down geometry in the following, $R_P = 0.180$); when starting from a contracted first-to-second Ag layer distance, Ag5 is found at a position 0.52 Å above (noted Ag5-up geometry in the following, $R_P = 0.185$). For a detailed comparison of all atom positions resulting from these optimizations, we refer to Table I. We note that the obtained height of the Ag5 atom opposes the height of the first layer in the starting geometry, indicating a nontrivial displacement of the surface Ag atoms during the search.

Triggered by this lack of sensitivity with respect to the position of Ag5, we also explored the possibility that this atom is missing completely, i.e., the PTCDA molecule would sit on a vacancy of the top Ag-layer. Such a model is in line with the adsorption geometry of C_{60} on the Ag(111) surface found by Li *et al.* [39,40], which includes an Ag vacancy below the molecule. Indeed, removing the Ag5 atom in the starting geometry led to a molecular geometry that is again similar to the former Ag5-down geometry and an even (by 5.4%) smaller R_P factor of 0.171. We note that when optimizing this geometry, the four Ag atoms surrounding the vacancy were allowed to relax laterally in accordance with the symmetry of the molecule, which contributed significantly to the decrease of R_P.

We also tested geometries with only 50% vacancies and with extra Ag ad-atoms resulting from the vacancy formation

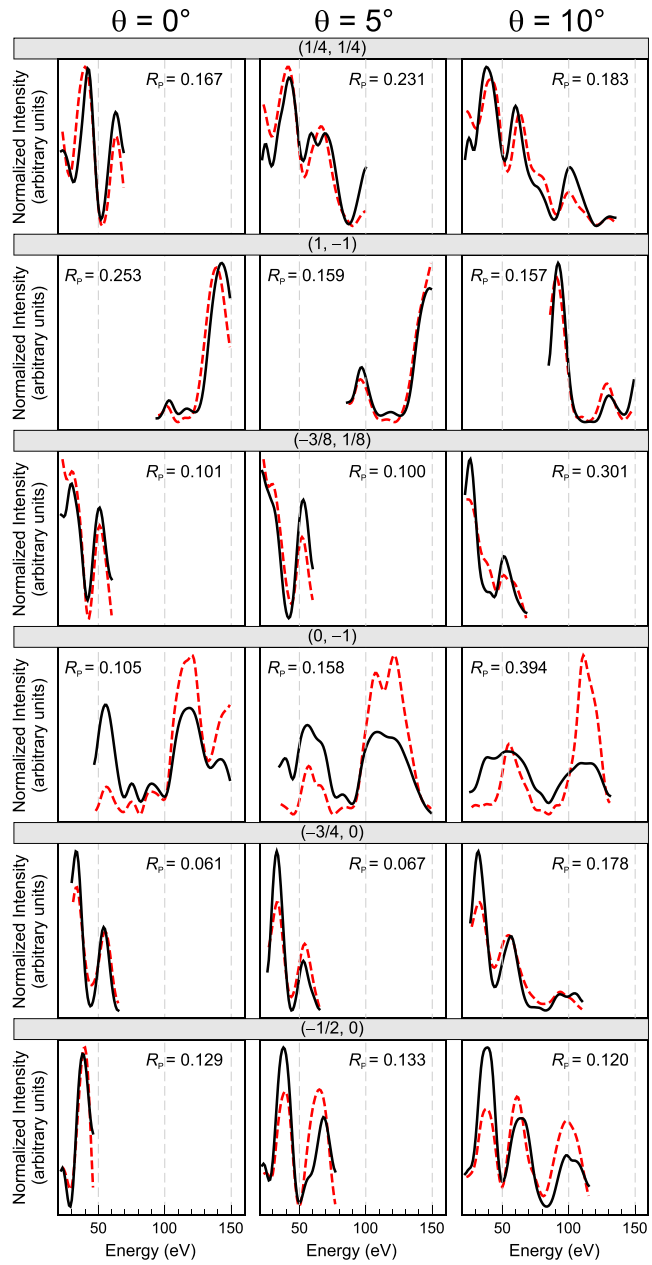

FIG. 5. Experimental (black) and theoretical (red) LEED-IV curves for PTCDA/Ag(100) of selected spots for three angles θ of beam incidence. The theoretical curves belong to the favored Ag-down model. The Pendry R_P factor is given for the individual curves. The overall value of R_P is 0.180. All curves were normalized by their respective integrals. For the complete set of all curves, see Ref. [25].

within the unit cell. The former was implemented in the model calculations by removing only one of the two Ag5 atoms underneath the two PTCDA molecules in the unit cell [see Fig. 4(b)]. This breaks the *p*4*gm* symmetry and, hence, the calculated IV curves had to be averaged over two domains. The resulting R_P factor of 0.198 is clearly outside the 8.4% error margin of the R_P achieved for the Ag5-down and Ag5-vacancy geometries. For the ad-atom + vacancy geometry, the additional ad-atoms were placed on the on-top positions

TABLE I. Adsorption heights of individual atoms of PTCDA and Ag atoms of the first and second Ag layers for three models optimized by LEED-IV and two optimized by DFT. All numbers, unless stated otherwise, are given in Å angstrom. In all three models, the PTCDA molecule sits on the on-top site [cf. Fig. 2(a)]. The model for the Ag5 atom moving up (Ag5-up) was not stable in DFT and is hence not included in the DFT column. In the DFT column, the adsorption energies ($E_{\mathrm{ad}}^{0\ \mathrm{K}}$ calculated at $T = 0$ K), the internal energies of adsorption $U_{\mathrm{ad}}^{300\ \mathrm{K}}$, and the free energies of adsorption $F_{\mathrm{ad}}^{300\ \mathrm{K}}$ (the latter two calculated at $T = 300$ K) are given. The last column contains the data from the NIXSW analysis reported in Ref. [1]. The numbering of atoms is according to Fig. 4. The second row lists the Pendry R factors (R_{P}) of the three models. The heights of the PTCDA atoms and Ag atoms determined by LEED-IV (at 120 K) and DFT are referenced to the averaged height d_0 of the atoms in the first Ag layer (Ag surface layer) defined as 0 Å. For an illustration see also Fig. 6 below. The heights from NIXSW refer to the position of the extended Bragg plane due to experimental reasons. The Ag surface first-to-second layer distances (referring to averaged heights) for the Ag-up, Ag-down, and vacancy geometries are 1.986, 1.949, and 1.948 Å. The second-to-third layer distances are 1.999, 2.057, and 2.097 Å. As a consequence, the position of the extended Bragg plane for the favored Ag-down model is located 0.079 Å above the average height of the Ag atoms of the first Ag layer. For a summary of the error bars of the LEED-IV analysis, we refer to Appendix F.

					DFT		
		LEED-IV			Ag5-down	Ag5-vacancy	
					$E_{\mathrm{ad}}^{0\ \mathrm{K}} = -4.05$ eV	−4.03 eV	
atom		Ag5-up	Ag5-down	Ag5-vacancy	$U_{\mathrm{ad}}^{300\ \mathrm{K}} = -4.07$ eV	−4.01 eV	
	R_{P}	0.185	0.180	0.171	$F_{\mathrm{ad}}^{300\ \mathrm{K}} = -3.74$ eV	−3.92 eV	NIXSW
O_{carb}	1	2.451	2.536	2.491	2.494	2.508	2.53
O_{anhyd}	2	2.674	2.755	2.697	2.657	2.665	2.78
C_{func}	3	2.507	2.566	2.550	2.668	2.657	2.73
C_{core}	4	2.729	2.815	2.768	2.799	2.737	2.84
	5	2.754	2.806	2.787	2.790	2.708	2.84
	6	2.671	2.727	2.687	2.846	2.704	2.84
	7	2.871	2.957	2.904	2.849	2.748	2.84
	8	2.736	2.820	2.734	2.900	2.739	2.84
	9	2.830	2.860	2.874	2.904	2.729	2.84
First Ag layer	1	0.100	0.140	0.137	0.034	0.054	
	2	0.019	0.058	0.058	0.079	0.077	not available
	3	−0.174	−0.138	−0.163	−0.105	−0.114	
	4	−0.027	−0.027	−0.056	−0.037	−0.048	
	5	0.522	−0.185	(vacant)	−0.071	(vacant)	
	6	−0.006	0.044	0.040	0.040	0.029	
	7	−0.095	−0.017	−0.046	−0.072	−0.085	
Second Ag layer	1	−2.022	−1.979	−1.972	−2.007	−2.003	not available
	2	−1.979	−1.951	−1.965	−2.025	−2.021	
	3	−1.988	−1.944	−1.941	−2.033	−2.003	
	4	−1.954	−1.923	−1.914	−1.977	−1.968	

between four terminal C = O groups of four PTCDA molecules in accordance with the symmetry, i.e., on the site given by the Ag atom number 1 in Fig. 4. An illustration of this model is given in Appendix D. This model led to an even higher R_{P} factor of 0.200 and can thus also be dismissed. We note that we had no evidence for the presence of Ag ad-atoms from STM images [12] or XPS data [1].

In summary, incomplete vacancy models with or without Ag ad-atoms can be ruled out on the grounds of their R factors, which are outside the 8.4% margin of the minimum $R_{\mathrm{P}} = 0.171$ ($0.171 + 8.4\% = 0.185$). But none of the three geometries listed in Table I, Ag5-up, Ag-down, and Ag-vacancy, can be excluded straightaway, as their R factors (0.185, 0.180, and 0.171, respectively) are all within each other's error margin.

In order to narrow down the true geometry, DFT calculations were thus performed for all three candidate models. Out of the two nonvacancy models, a stable energy minimum could only be found for the Ag5-down geometry, but not for Ag5-up. Therefore the latter can be dismissed right away. We will comment on the reasons for this minimum for the R_{P} factor for the Ag5-down geometry in the discussion section.

In order to discriminate between the Ag5-down and the Ag5-vacancy geometries, we took a closer look at the adsorption energies calculated by DFT (at 0 K in the first step). These are almost identical, $E_{\mathrm{ad,\,Ag5\text{-}down}}^{0\ \mathrm{K}} = -4.05$ eV versus $E_{\mathrm{ad,\,Ag5\text{-}vac}}^{0\ \mathrm{K}} = -4.03$ eV, when PTCDA is adsorbed on the Ag(100) surface without and with a given vacancy site, respectively. We note that in an earlier study [1], we calculated the adsorption energy for Ag5-down at PBE-D3 level as −4.2 eV, which compares well to the present value of −4.05 eV, given that different functionals were used. The same agreement applies to the structural coordinates. The present calculation gave a slightly larger height of the perylene core (+0.05 Å) and smaller heights of the carboxylic O (O_{carb}) and anhydride O (O_{anhyd}) atoms (−0.04/ − 0.05 Å), which yields a larger distortion of the molecule. A detailed comparison is provided in Appendix E.

The small difference between $E^{0\,K}_{ad,\,Ag5\text{-}down}$ and $E^{0\,K}_{ad,\,Ag5\text{-}vac}$ is plausible as the loss in interaction energy between the missing Ag5 atom and the PTCDA in the vacancy geometry is compensated by the elastic energy related to the distortion of the Ag surface by the downward move of the Ag5 atom in the down geometry.

Clearly, for a proper comparison of the energies, we also need to take into account the vacancy formation energy on Ag(100). This has been calculated at 0 K to be $E^{0\,K}_{Ag,\,vac} = 0.37$ eV by Liu [41]. In this calculation, the Ag atom expelled from the surface is readsorbed at a kink site of a Ag island. Alternatively to the formation on a terrace, the vacancy could be formed at a kink site of a Ag terrace edge, which is followed by a subsequent diffusion of the vacancy into the upper terrace [41]. Adding $E_{Ag,\,vac}$ to $E^{0\,K}_{ad,\,vac}$ leads to a very significant energy difference of 0.39 eV in favor of the Ag5-down geometry versus the vacancy geometry.

For additional safeguarding these conclusions from DFT calculations, we have also included finite temperature effects at 300 K and computed the internal energy $U^{300\,K}_{ad}$ and the free energy of adsorption $F^{300\,K}_{ad}$ at 300 K for both geometries. These values are included in Table I. The vibrational energy and the entropy included in the free energy at a finite temperature ($F^{300\,K}_{ad} = U^{300\,K}_{ad} - 300\text{ K} \times S^{300\,K}_{ad}$) turn the difference between the free energies in favor of the vacancy site. This is now preferred by 0.18 eV versus the Ag5-down geometry at 300 K ($F^{300\,K}_{ad,\,Ag5\text{-}vac} = -3.92$ eV versus $F^{300\,K}_{ad,\,Ag5\text{-}down} = -3.74$ eV). This is remarkable and demonstrates that thermal effects have to be included in DFT calculations at this level of accuracy for organic molecules like PTCDA. However, the total energy gain upon adsorption is still larger for the Ag5-down geometry, because the difference of 0.18 eV is too small to compensate the energy $E^{0\,K}_{Ag,\,vac} = +0.37$ eV that is required for generating the vacancy in the Ag surface [-3.74 eV $<$ $(-3.92 + 0.37)$ eV].

We also asked ourselves whether a finite temperature effect could reduce the energy for the vacancy formation of the Ag surface considerably, and thus turn the balance. Hence, we calculated the internal energy $U^{300\,K}_{Ag,\,vac}$ and the free energy $F^{300\,K}_{Ag,\,vac}$ for the vacancy formation at a finite temperature of 300 K. Likewise, as Liu [41], we computed the quantities from the difference in U and F between a surface with a kinked step and the same surface with an additional vacancy on a terrace plus a Ag adatom placed at a former kink site of a terrace edge. We obtained $U^{300\,K}_{Ag,\,vac} = +0.37$ eV and $F^{300\,K}_{Ag,\,vac} = +0.36$ eV. The value of $U^{300\,K}_{Ag,\,vac}$ is in remarkable agreement with $E^{0\,K}_{Ag,\,vac} = +0.373$ eV calculated by Liu [41]. We suppose that this agreement of $U^{300\,K}_{Ag,\,vac}$ and $E^{0\,K}_{Ag,\,vac}$ (from Liu) results from the mutual cancellation of effects due to the use of different basis sets, different methods, and the included temperature related contributions. Moreover, the difference between $U^{300\,K}_{Ag,\,vac}$ and $F^{300\,K}_{Ag,\,vac}$ is only very small (0.01 eV). This is different from what was found for the respective energies referring to the adsorption of the PTCDA molecule, where the difference between $U^{300\,K}_{ad}$ and $F^{300\,K}_{ad}$ for the Ag-down geometry was -0.33 eV, demonstrating the role of entropic contributions for the adsorbate. In conclusion, on the basis of DFT calculated free energies at 300 K, the Ag5-down geometry is preferred over the Ag5-vacancy geometry by 0.18 eV. Decisive is the energy needed for the creation of the vacancy.

TABLE II. Summary of the most important structural parameters obtained for the Ag-down model. All values are given in angstroms. The heights are referenced as in Table I. For the numbering of the atoms see Fig. 4(a). The height of C_{core} is the average height of the C atoms of type (4) to (9). Additionally, the molecular vertical distortion, the height difference between the O_{carb} and O_{anhyd} atoms, and the maximum to minimum height values of the first and second Ag layers (buckling) are given. Note, for NIXSW, the molecular distortion is the height difference between C_{core} and O_{carb}, while for LEED-V and DFT, it refers to the height difference of the C atom in the core that is farthest away from the substrate to O_{carb}.

	LEED-IV	DFT	NIXSW
O_{carb} (1)	2.54	2.49	2.53 ± 0.02
O_{anhyd} (2)	2.76	2.66	2.78 ± 0.02
C_{func} (3)	2.57	2.67	2.73 ± 0.01
C_{core}	2.82	2.85	2.84 ± 0.02
molecular distortion	0.42	0.41	0.31 ± 0.03
$\Delta(O_{anhyd}/O_{carb})$	0.22	0.16	0.25 ± 0.04
buckling first Ag layer	0.33	0.18	not avail.
buckling second Ag layer	0.06	0.06	not avail.

One may argue that a sufficient number of vacancies are present on the bare surface in thermal equilibrium at 300 K, similar to ad-atoms, and that these could be trapped underneath PTCDA molecules adsorbed on the surface. However, we find it difficult to envisage such a scenario because, experimentally, we find that the formation of the ordered PTCDA structure occurs spontaneously upon deposition at room temperature without further annealing. In addition, we did not observe any features in the diffusion of PTCDA molecules [42], nor in the island decay of PTCDA on Ag(100) [43], which could indicate the presence of vacancies.

Therefore the Ag5-vacancy geometry must be dismissed on the grounds of the energy considerations and the given experimental observations, even though its R factor is slightly lower.

B. Molecular distortions of PTCDA

All atomic adsorption heights of the PTCDA molecule and the Ag atoms in the first and second Ag layer obtained for the Ag-down model by LEED-IV are listed in Table I. For comparison, we also include the respective data from DFT and NIXSW. For LEED-IV and DFT, the heights are referenced to the averaged height of the first Ag layer d_0, which is set to 0 Å. This is reasonable, as the R factor and the energies calculated by DFT are most sensitive to the atomic distances of the molecular atoms to the first Ag layer. However, for experimental reasons, heights measured by NIXSW are always referenced to the position of the extended Bragg plane. Accordingly, they are given in Tables I and II. The position of the extended Bragg plane to the first Ag layer d_{Bragg} is calculated from the LEED-IV results by subtracting two times the ideal lattice spacing from the sum of the obtained first-to-second layer and second-to-third layer distances. This yields $d_{Bragg} = +0.079$ Å (see also Table I).

A schematic illustration of the vertical atomic heights obtained by the different methods is given in Fig. 7 below. Again, the heights from LEED-IV and DFT are referenced to the averaged height of the first Ag layer; the heights from NIXSW are against the extended Bragg plane. For referencing the heights determined by NIXSW against the average height of the atoms in the first Ag layer (d_0), as determined from LEED-IV, a distance of 0.079 Å would have to be added. However, this is not done for the intended comparison, because the position of the Bragg plane derived from LEED-IV can be subject to a larger uncertainty for the following reason. The Bragg plane is defined with respect to the heights of the atoms in the third Ag layer. These are considered to be located at their bulk positions in the LEED-IV analysis. However, these positions deeper in the bulk are typically subject to larger errors in LEED-IV, due to the attenuation of the diffracted electrons. As a consequence, the position of the calculated Bragg plane suffers from the same error.

The Ag-down geometry determined from LEED-IV is illustrated in Fig. 6 with a top and two sectional views along the short and long sides of the molecule. Table II summarizes the most important structural parameters and will be used in our following description of the adsorption geometry. We find an archlike adsorption conformation of the PTCDA molecule with an overall minimum to maximum distortion of 0.42 Å (NIXSW 0.31 Å and DFT 0.41 Å). The carboxylic O atoms (O_{carb}) are closest to the substrate, the C7 (DFT C9) atoms in the perylene core are farthest away from the substrate, and the anhydride O atoms (O_{anhyd}) are at intermediate positions. Both the O_{carb} and the O_{anhyd} atoms come close to Ag top sites (see Fig. 6).

There is a prominent height difference between the O_{carb} and the higher O_{anhyd} atoms [$\Delta(O_{anhyd}/O_{carb})$ in Table II]. It comes out at 0.219 Å (NIXSW 0.25 Å and DFT 0.163 Å). The perylene core (comprised of four outer and one central benzene ring) is nonplanar. The distortion in the outer four benzene rings, between the C6 (pink/lowest) on an Ag bridge site and the C7 atom (violet/highest) on an Ag top site amounts to 0.230 Å. As a result, the molecule exhibits the shape of an upside-down "V" and "W," when viewed from its short and long sides, respectively [see Figs. 6(b) and 6(c)]. For the C_{func} atoms (C3), which are located close to Ag bridge sites, LEED-IV finds a height close to that of the O_{carb} atoms, while DFT and NIXSW indicate a height closer to that of the O_{anhyd}.

As mentioned above, the change in the lateral molecular coordinates was modeled by a symmetric stretch of the molecule. We found only very small deviations from the preset lateral geometry for all tested geometries of the order of +0.5 to 1%. These values are smaller than the respective error bars of the LEED-IV analysis and are thus not meaningful. For example, for the favored Ag5-down geometry, we found a small stretching of the molecule along the long axis by $1.0\% \pm 1.4\%$. Hence, within the resolution of our LEED experiment, we can state that the molecule maintains its lateral footprint on the surface. However, deviations of individual bond lengths from those in the gas phase are, of course, still possible and likely, while the overall footprint is preserved.

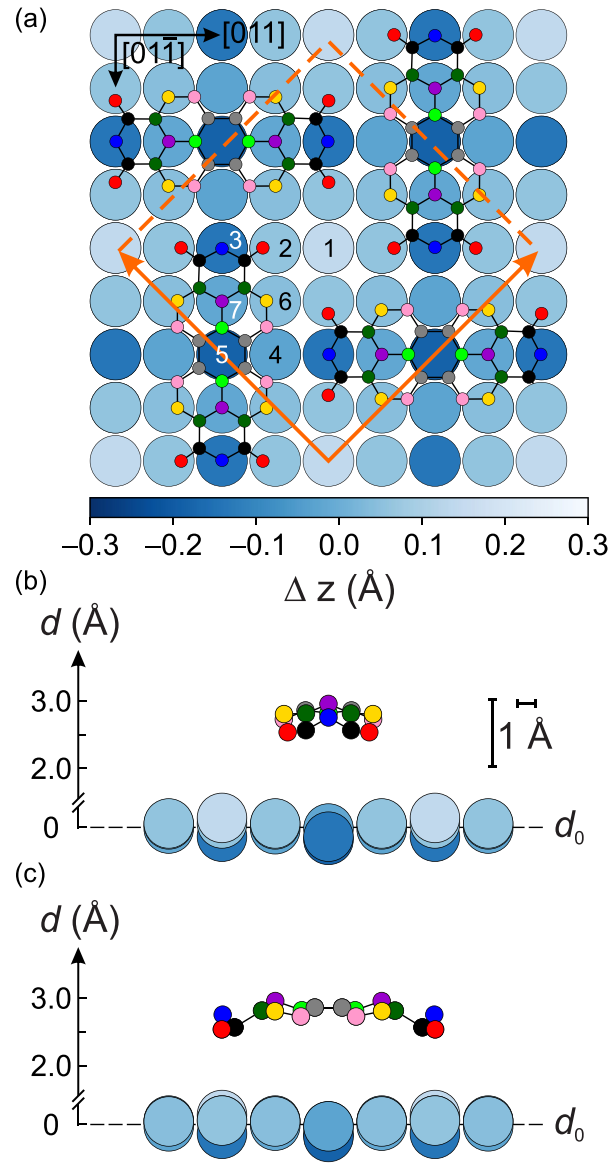

FIG. 6. Top (a) and sectional views [(b) and (c)] along the short and long axes of PTCDA for the Ag-down adsorption geometry (Ag-down model) as derived from LEED-IV. Ag atoms are shown in different shades of blue to indicate the vertical deviation from the averaged height of the first Ag layer (dashed line at height d_0). O_{carb}/O_{anhyd} in red/blue and the chemically different C atoms marked by different colors as in Figs. 4 and 7. The numbers mark specific Ag atoms in the first Ag layer as done in Fig. 4. In the side views, d denotes the vertical positions and is referenced against d_0, i.e., the averaged height of the Ag atoms in the first Ag layer. (We note that this is different to Fig. 1 in Ref. [1], where the heights were referenced against the extended Bragg plane d_B.) For better visibility of the molecular distortion and substrate buckling, the intermolecular distances and the buckling of the Ag substrate with respect to the averaged height values of the PTCDA atoms and the Ag substrate atoms, respectively, are enlarged by a factor of 4.

C. Buckling and relaxation of the Ag(100) surface

We find a significant buckling ($z_{max} - z_{min}$) for both the first and the second Ag layer of 0.33 Å and 0.06 Å (DFT 0.18 Å/0.06 Å), respectively. The "uncovered" Ag1 atom in

the center of the unit cell is the highest, the Ag5 atom below the center of the molecule is the lowest, and the Ag3 atom below the O_{anhyd} is the second lowest. Overall, we find a cross-shaped depression pattern in the Ag substrate centered on the molecule [see Fig. 6(a)]. It is reproduced to a good extent by the present DFT calculation and the earlier one [1]. In comparison to the clean surface (for details we refer to Appendix B), the first-to-second layer distance is further contracted upon adsorption by 0.074 Å (2.023 Å → 1.949 Å) yielding a total contraction of 0.094 Å while the second-to-third layer distance expands by a small amount of 0.024 Å (2.033 Å → 2.057 Å) and is by 0.014 Å slightly larger than the ideal layer spacing (2.043 Å). As a result, the top Ag layer is 0.079 Å below the position of the extended Bragg plane for the PTCDA-covered surface, while it is 0.039 Å below for the clean surface (taking into account the first four layer distances determined by LEED-IV, see Appendix B).

VI. DISCUSSION

We start the discussion by commenting on aspects of the methodology before considering the insight into the chemical bonding that is gained. Importantly, the LEED-IV analysis confirms the adsorption site and distortion of the molecule, which was found in NIXSW experiments before. The fourfold hollow site could be clearly dismissed at an early stage of the optimization. This is an important result that benchmarks the LEED-IV method. Both LEED-IV and DFT show qualitatively very similar distortions of the molecule and the Ag layers, although quantitatively, those determined by LEED tend to be larger. The *R* factors which we obtain are rather small (less than 0.2), and we consider them as meaningful, as we have provided a reasonable energy range of 200 eV/per optimized parameter by using different angles of incidence. This demonstrates that LEED-IV is capable of finding the correct adsorption site and geometry for molecular structures with large unit cells, even if the maximum energy is restricted by the experiment, as in this case.

Probably the most puzzling finding is that the LEED-IV analysis appears to be rather insensitive to the Ag5 atom, which is located below the center of the molecules. This is the reason why we could not identify the correct adsorption geometry on the basis of the *R* factor minimum alone, but only in combination with DFT. There are several potential reasons for this shortcoming of the LEED-IV analysis. Most importantly, there are only two Ag5 atoms in the $c(4 \times 4)$ unit cell, which consists of 32 Ag atoms in the first layer. The other types of Ag atoms, except Ag1, represent four or even eight symmetry equivalent atoms in the same unit cell. Therefore the contribution of the Ag5 atom to the overall diffraction signal is relatively small. This is probably exacerbated by the fact that Ag5 – unlike Ag1 – is covered by the molecule, and thus its back-scattered electron signal is more strongly attenuated. The indifference between the Ag-up and Ag-down geometries is probably also related to the well-known problem of LEED-IV that false *R* factor minima appear when an atom is moved by half the average de Broglie wavelength of the energy range used in the analysis. The height difference of Ag5 between the two geometries is around 0.71 Å, which is very close to half the average wavelength of 0.74 Å of our analysis.

This ambiguity of the structure determination in our present LEED-IV analysis could possibly be lifted if a data set spanning an even wider energy range were available. However, for higher energies, the spots were too weak and too dense on the screen to be discriminated from each other. In addition, the large size of the supercell makes the model calculations very expensive for high energies. Both limitations require further experimental and computational effort. It is important to note, however, that all structure parameters other than the height (or presence) of Ag5 are very similar between the three structures listed in Table I and can, therefore, be considered reliable.

As noted in the introduction, the bonding of PTCDA to different metallic [1], passivated [44,45], or even wide band gap material surfaces [46] has been compared with the intention to identify principles of the interfacial bonding. For a more complete discussion on this topic, we refer to Ref. [1]. Here, we recapitulate the most important features and will discuss the bonding in view of the novel findings made here. Due to electron donation, the former LUMO (lowest unoccupied molecular orbital) of the PTCDA is partially filled. This gives the electron density of the adsorbed molecule a more quinoidal character compared to the isolated molecule and leads to charge accumulation on the terminal O_{carb} atoms [1]. These O atoms are attracted to the surface and bend downwards because the central perylene core feels repulsive interactions at this reduced height and cannot follow the downward move of the O_{carb} atoms due to Pauli repulsion. This applies in particular to the region, where the nodal plane of the former LUMO is located, and where the electron density of the metal/molecule hybrid state is marginal, i.e., underneath the long central axis of the PTCDA molecule [1]. As a result, the PTCDA molecule exhibits an archlike geometry on the Ag(100) surface, along the long and short directions, where the carboxylic O atoms are closest to the substrate and the perylene core is further away. This picture is fully confirmed by the present LEED-IV analysis. However, to keep the picture complete, we recall that the molecular geometry is not only determined by the interfacial bonding but also by intermolecular interactions, which are established by hydrogen bonds between the carboxylic O atoms and H atoms on the periphery of the perylene core of the next-neighbored molecule (see Fig. 2). These pull the carboxylic O atoms laterally and thus counteract to some extent the vertical Ag–O bonds.

The LEED-IV analysis adds further important aspects to the understanding of this picture of bonding of PTCDA to the Ag(100) surface. First, we find that the perylene backbone is not uniformly bent but vertically distorted in the sense of a buckling on the length scale of bonds between the atoms. Such a buckling of the backbone was not unexpected but could not be proven experimentally so far. For instance, the different C atoms in the backbone could not be discriminated in the NIXSW analysis because their photoemission peaks could not be separated at the required higher photon energies [1]. As said above, the atoms C7 (located on an Ag on-top site) are at the largest height (2.96 Å), and the C_{func} (C3) atom (located approximately on a bridge site) is at the

lowest height (2.57 Å). Hence, the C atoms in the central ring (C8 and C9) are not at the highest position, as would be expected for a uniform and homogeneous archlike bending of the molecule. Rather, local and different interactions between individual C and Ag atoms play a role and cause the vertical distortions within the backbone. Evidently, these distortions of the π system will have an impact on the valence orbitals of the adsorbed molecule, and these distortions on the Ag(100) surface are expected to be different from those of PTCDA adsorbed on the other Ag surfaces of different orientations, i.e., (111) and (110). For instance, smaller vertical distortions of the C atoms on the perylene core are expected on Ag(111) in correlation with a weaker bonding and hybridization of the valence band orbitals with the Ag states, similar to the trend of the distortion that is seen for the heteroatoms [45,47].

The second new aspect concerns the vertical distortion of the first Ag layer due to the adsorption of the molecule. This was discussed already in detail in Ref. [1] on the basis of DFT results. However, now these details are proven experimentally and allow interesting conclusions. Most important in the interfacial bonding are the O_{carb} atoms. These come close to the substrate, approximately at an on-top position with respect to the Ag2 atom (cf. Fig. 7). This is reflected by its upward move of 0.06 Å with respect to the averaged height of the Ag surface atoms. Indeed, the Ag2 atom in the first layer is the second-highest one, after the uncovered Ag1 atom. Hence, the local bond between the O_{carb} atoms and the Ag2 atoms is directly evidenced by the vertical displacements of the Ag surface atoms and the resulting short bond distances. The O_{carb} atoms pull the Ag2 atoms out of the surface. We propose that these bonds between the Ag2 atoms and the O_{carb} atoms favor the top site of the molecule over the alternative hollow site because for the latter the O_{carb} would come close to a bridge site, which is presumably unfavorable for the formation of local bonds to the O_{carb} atoms (cf. Fig. 2).

The Ag atoms 4 and, in particular, 5 (cf. Fig. 7), which are next and at the center of the molecule moved to positions that are by 0.03 and 0.19 Å below the averaged height of the first Ag layer. This demonstrates the noted repulsive interaction between the center of the perylene and the Ag surface. All six C atoms of type C8 (2×) and C9 (4×), which comprise the central benzene ring, encircle the Ag5 atom and push it into the substrate in a concerted manner. From the distortion pattern of the Ag surface, we can thus verify the picture of attractive bonds via the four O_{carb} atoms and a repulsive interaction on the perylene core in full agreement with the earlier discussion given in Ref. [1].

The observed buckling of the Ag surface, i.e., the first Ag layer, by 0.33 Å is rather significant. For comparison, LEED-IV reveals that glycine on Cu(110) leads to a buckling of 0.07 Å [4]. A local lifting of individual Cu substrate atoms due to a covalent bond to heteroatoms in a π-conjugated molecule was also found for trithiolate on Cu(111) by LEED-IV [7]. There, the Cu atoms below the sulfur atoms were found to be lifted upward by 0.10 Å due to local bonds to the S atoms, similar to the (although smaller) lifting of the Ag atoms (0.06 Å) that are located below the carboxylic O atoms in the present case.

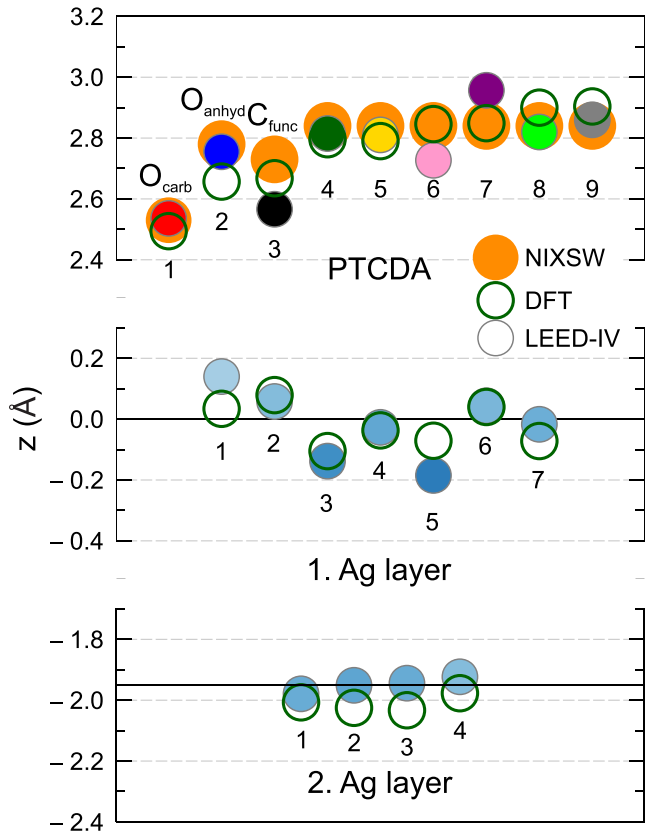

FIG. 7. Comparison of adsorption heights of atoms obtained from LEED-IV, DFT, and NIXSW for the favored Ag-down geometry from Table I. The atoms of the PTCDA are numbered according to Fig. 4 and Table I. The Ag atoms are numbered according to Fig. 6(a). The atom positions from LEED-IV are marked by different colors with the same color coding as in Fig. 6(a). Positions from NIXSW (only PTCDA atoms) are marked by the orange-filled circles; positions from DFT are marked by the open green circles. Note that the lateral arrangement is without meaning. The solid horizontal lines mark the averaged heights of the first and second Ag layers.

Evidently, vertical displacements of the substrate atoms contribute strongly to the intensity of the superstructure spots in the respective LEED patterns, as they are much stronger scatterers than the light molecular atoms. However, this conclusion is possibly less valid concerning the Ag5 atom below the symmetry center of the PTCDA, which was found to have only a small impact on the R factor. Concerning the discussion of the absence of this atom and the presence of an Ag vacancy, there exists an interesting similarity with the LEED-IV/DFT analysis reported for C_{60}/Ag(111) by Li *et al.* [39,40]. The authors concluded in favor of the vacancy, on the basis of both the R factors [$R_P = 0.42$ (top site) versus 0.36 (vacancy site)] and the adsorption energies from DFT calculations [$E_{ad} = -1.27$ eV (top site) versus -1.94 eV (vacancy including the formation energy E_{vac})]. By contrast, for PTCDA/Ag(100) the Ag-down and the vacancy geometries lead to nearly indifferent R_P factors (0.180 versus 0.171), and only based on the DFT calculations, the down geometry is favored from its lower free energy of adsorption over the vacancy geometry [-3.74 eV versus -3.56 eV =

$(-3.92 + 0.36)$ eV for 300 K]. The two adsorption scenarios can possibly be understood from the different footprints of the molecules: For C_{60} only one hexagonal ring is in contact with the Ag(111) surface, and the vacancy formation after annealing to 675 K allows an optimized local bonding of the six C atoms to the Ag surface atoms. For PTCDA, the contact to the Ag surface is via both the perylene core and the terminal carboxylic O groups, and the energy gain due to a vacancy formation is thus smaller. This may indicate that vacancy formation is not a common aspect for planar organic molecules.

VII. CONCLUSIONS

From a LEED-IV analysis, we were able to verify the formerly determined adsorption site of PTCDA on the Ag(100) surface. An important aspect was that we used a large data set of LEED-IV curves, spanning a large total energy range, which was achieved by including different angles of incidence to compensate for the rather low high-energy limit that is given by the large unit cell and the resulting high density of spots on the LEED screen. The high-symmetry fourfold on-top adsorption site, which was obtained from NIXSW experiments earlier, was verified by its significantly smaller *R* factor with respect to the alternative fourfold hollow adsorption site. The vertical out-of-plane distortions of the terminal carboxylic O (O_{carb}) and C atoms (C_{func}) and the anhydride O atoms (O_{anhyd}) are found in good agreement with earlier results from NIXSW and new results from DFT calculations. However, for the carbon atoms within the central perylene core, the out-of-plane distortions could be determined experimentally for the first time by LEED-IV because these C atoms could not be spectroscopically resolved in the NIXSW experiments.

In addition, our LEED-IV analysis provided the vertical reconstruction, i.e., the buckling of the Ag surface for the first time. This knowledge completes the understanding of the chemical bonding of PTCDA to the Ag(100) surface because the reconstruction of the surface is, so to speak, the counterpart to the distortion of the molecule. We also note that concerning the depression or even absence of the Ag atom below the center of the perylene core (i.e., the Ag atom that actually defines the on-top site) the LEED-IV analysis had a certain blind spot as it could not discriminate between the situations of a depressed and a missing Ag atom from the *R* factor alone, and, hence, had to be aided by DFT calculations. The reason for this ambiguity is not fully clear and deserves further attention.

Regarding the methodology, our work can be understood as a showcase for the ability and limitations of LEED-IV for the analysis of such adsorbate systems. The presented results motivate further studies of π-conjugated, or larger organic molecules with functional groups in general, on this and other substrates, by LEED-IV. The method is in particular attractive when structural data cannot be achieved by NIXSW, or other structural methods, i.e., photoelectron diffraction, due to experimental limitations, e.g., on insulator surfaces, which are rapidly destroyed by the intense x-ray beam, but which may allow LEED-IV measurements if means for charge compensation are taken.

ACKNOWLEDGMENT

Financial support by the German Research Foundation (DFG) under the Grant No. So407/6-3 and via the Collaborative Research Centre SFB-1083 (project A12) is acknowledged.

DATA AVAILABILITY

The data that support the findings of this article are openly available [48].

APPENDIX A: ILLUSTRATION OF THE SMALL AND LARGE UNIT CELLS OF PTCDA/Ag(100)

Figure 8 illustrates the small $p(4\sqrt{2} \times 4\sqrt{2})\mathrm{R}\,45^\circ$ unit cell (containing two molecules) which was used for the LEED-IV calculations in comparison with the larger $c(8 \times 8)$ unit cell (containing 4 molecules) which is commonly used for identifying the symmetry elements.

APPENDIX B: LEED-IV ANALYSIS OF THE CLEAN Ag(100) SURFACE

For the clean Ag(100) surface, the LEED-IV data set was recorded for one single angle of incidence, which was close to, but not exactly normal incidence. The electron energy ranged from 50 to 300 eV, and in total 16 spots belonging to 4 different diffraction orders were measured, yielding a total energy range of 2534 eV and an *RR* factor of 0.112. The sample temperature was kept at 180 K. For the structure search, we used the same computer code as for the PTCDA-covered surface. During the search procedure, the incidence angles θ and Φ were fitted and values $\theta = -1.26^\circ \pm 0.27^\circ$ and $\Phi = -105.9^\circ \pm 12.39^\circ$ were obtained.

An ideal bulk structure with lattice constant 4.085 Å was used as the start geometry for the search. No lateral displacements of the Ag atoms were considered, as these are incompatible with the symmetry of the surface; only variations of the layer distances between the first five layers were allowed. The maximum angular momentum quantum number ℓ_{max} was set to 8. The vibrational *rms* amplitudes were optimised at 0.05 and 0.03 Å for the first and all other Ag layers, respectively.

The best-fit Pendry *R* factor is $R_P = 0.120$, which is a significant improvement from the start geometry yielding $R_P = 0.343$. The best-fit structure is illustrated in Fig. 9, which also shows the inter-layer distances calculated from the obtained vertical positions.

The best fit shows small relaxations for the first four interlayer distances. In particular, we find a first to second Ag interlayer contraction of $\Delta d_{12} = -0.020 \pm 0.020$ Å, a second-to-third interlayer contraction of $\Delta d_{23} = -0.010 \pm 0.017$ Å, a third-to-fourth interlayer expansion of $\Delta d_{34} = +0.008 \pm 0.020$ Å, and a fourth-to-fifth interlayer contraction of $\Delta d_{45} = -0.017 \pm 0.028$ Å. The distance between

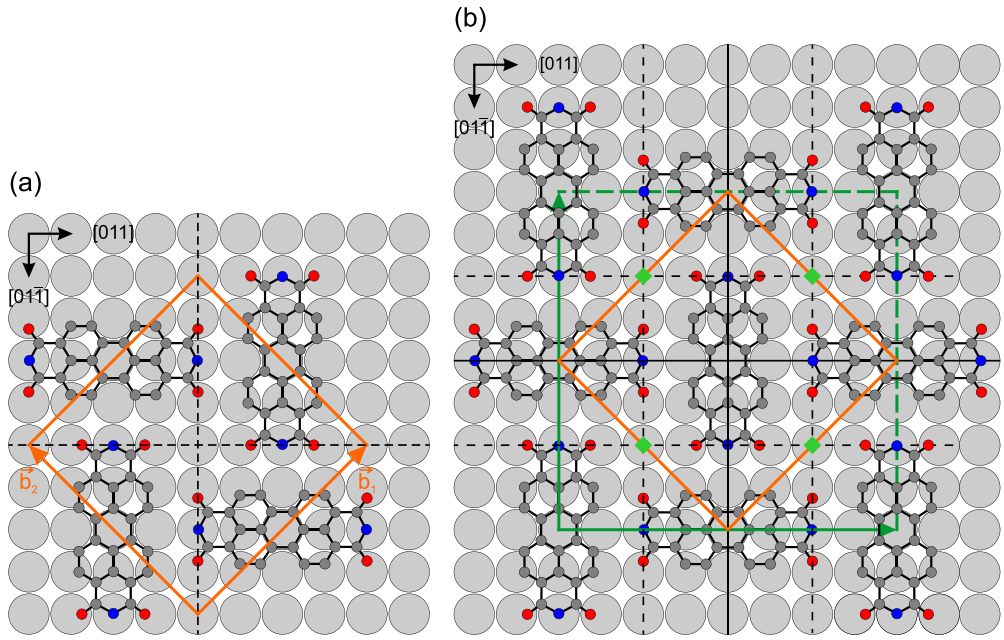

FIG. 8. Hardsphere models of the different unit cells for PTCDA/Ag(100). (a) $p(4\sqrt{2}\times 4\sqrt{2})\mathrm{R}\,45^\circ$ unit cell, (b) $c(8\times 8)$ unit cell. The dashed (full) lines (black) indicate the glide lines (mirror planes).

the topmost and the second layer has the largest relaxation of -0.98% compared to the ideal layer spacing of the bulk of 2.043 Å, while that of the second to the third layer is only half as large (-0.49%), followed by an expansion/contraction of the third-to-fourth and fourth-to-fifth layer distances ($+0.39\%$ and -0.8%).

To our knowledge, two investigations of the clean Ag(111) surface by LEED-IV have been reported, namely, by Li *et al.* [15] and by J. Wang in his PhD thesis [49]. Remarkably, Li *et al.* [15] claimed that no relaxation is present. However, we consider our result as more trustworthy because of the better R_P factor of 0.120 compared to that from Li *et al.* of $R_\mathrm{P}=0.39$, which is, in addition, higher than usually obtained R_P factors for clean surfaces. J. Wang obtained a more reliable value of $R_\mathrm{P}=0.15$ for their analysis of six spots [49]. Similar to us, they found $\Delta d_{12}=-0.025\pm 0.02$ Å and $\Delta d_{23}=-0.006\pm 0.03$ Å, while no modifications with respect to the bulk value were obtained for d_{34} and d_{45}. We judge these results to be consistent with ours within the given experimental accuracy. The small inward relaxations of the first and second layer distance of the order of 1% are also supported by theoretical calculations [50]. As an important consequence, the topmost layer of the clean surface is -0.039 Å below the position of the extended Bragg plane.

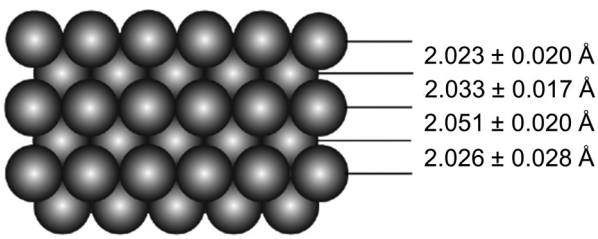

FIG. 9. Hardsphere model of the bare Ag(100) surface. Illustrating the vertical layer distances obtained of the LEED-IV analysis.

APPENDIX C: CALCULATION OF THE INTERNAL ENERGY U AND THE HELMHOLTZ FREE ENERGY F AT FINITE TEMPERATURES

For calculating the internal energy U and the Helmholtz free energy F at finite temperatures, we considered the thermal energies and zero point energies related to the phonons. Electronic excitations were not taken into account. We refer to a set of vibrational/phonon modes (ω_k), named as phonons in the following for brevity, with energies in harmonic approximation $\varepsilon(n)=(n+\frac{1}{2})\,\hbar\,\omega_k$, n being $0,1,\ldots$. The contribution of the phonons to the internal energy U and the Helmholtz free energy F from the computed ω_k was performed according to the following formulas. These can be found in textbooks on statistical thermodynamics, e.g., Ref. [51]; we summarize these for completeness. The following quantities refer to contributions of the phonons.

The partition function $Z(T)$ is given as

$$Z(T)=\sum_k\sum_n^{\infty}\exp\left(-\frac{\hbar\,\omega_k}{k_\mathrm{B}\,T}\,n\right)=\sum_k\frac{1}{1-\exp\left(-\frac{\hbar\,\omega_k}{k_\mathrm{B}\,T}\right)}. \tag{C1}$$

The internal energy $U(T)$ is related to $Z(T)$:

$$U(T)=k_\mathrm{B}\,T^2\left[\frac{\partial}{\partial\,T}\,Z(T)\right]. \tag{C2}$$

Adding the zero-point energies $\sum_k\frac{1}{2}\hbar\,\omega_k$ yields

$$U(T)=\sum_k\hbar\,\omega_k\left[\frac{1}{2}+\frac{1}{\exp\left(-\frac{\hbar\,\omega_k}{k_\mathrm{B}\,T}\right)-1}\right]. \tag{C3}$$

The entropy $S(T)$ is obtained from $Z(T)$ via Eq. (C1):

$$S(T) = k_B\, T \left[\frac{\partial}{\partial\, T}\, \ln\left(Z(T)\right)\right] + k_B \ln\left(Z(T)\right), \qquad \text{(C4)}$$

which yields

$$S(T) = \sum_k k_B \left[\frac{\hbar\,\omega}{k_B\, T}\, \frac{1}{\exp\left(\frac{\hbar\,\omega_k}{k_B\, T}\right) - 1} - \ln\left(1 - \exp\left(-\frac{\hbar\,\omega_k}{k_B\, T}\right)\right)\right]. \qquad \text{(C5)}$$

From Eqs. (C3) and (C5), the Helmholtz free energy $F(T)$ is obtained as $F(T) = U - T\,S(T)$.

For obtaining the internal and free energies of the total system, which further includes the electronic contributions, the above calculated contributions of the phonons [noted from now on by $U_{ph}(T)$ and $F_{ph}(T)$] to $U(T)$ and $F(T)$ were added to the internal energy $U^{0\ \mathrm{K}}$ calculated at $T = 0$ K:

$$U^{300\ \mathrm{K}} = U^{0\ \mathrm{K}} + U_{ph}^{300\ \mathrm{K}} \quad \text{and} \quad F^{300\ \mathrm{K}} = U^{0\ \mathrm{K}} + F_{ph}^{300\ \mathrm{K}}. \qquad \text{(C6)}$$

The adsorption energies ($U_{ad}^{300\,\mathrm{K}}$ and $F_{ad}^{300\,\mathrm{K}}$) were finally computed from the differences of $U^{300\ \mathrm{K}}$ and $F^{300\ \mathrm{K}}$ of the products (adsorbed molecule on the surface) and reactants (bare surface plus molecule in the gas phase). The same was performed for the calculation of $U_{\mathrm{Ag,\,vac}}^{300\,\mathrm{K}}$ and $F_{\mathrm{Ag,\,vac}}^{300\,\mathrm{K}}$ of the Ag vacancy.

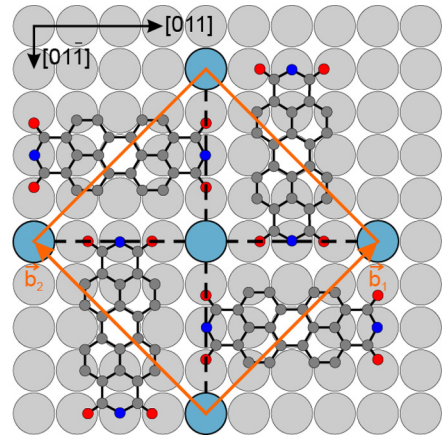

FIG. 10. Hardsphere model of the vacancy plus Ag-ad-atom model of PTCDA/Ag(100). Note the four missing Ag5 atoms in the topmost surface layer below the central bencene ring of the molecule. These atoms are found as ad-atoms (blue color) on on-top positions between four carboxylic O atoms.

APPENDIX D: ILLUSTRATION OF THE VACANCY MODEL OF PTCDA/Ag(100)

In Fig. 10, we show the hardsphere model of the vacancy structure with the Ag ad-atoms that was considered for LEED-IV calculations and gave an R_p factor of 0.200.

APPENDIX E: COMPARISON OF DFT CALCULATED PARAMETERS TO EARLIER CALCULATED ONES

Table III compares DFT calculated structure parameters from an earlier and the present calculation.

TABLE III. Comparison of DFT calculated structural parameters for the Ag-down model, similar to Table II, from our earlier DFT calculation [1] and the DFT calculation of the present work. All values are given in sign. The same definitions as for Table II apply. However, different from Table II, the molecular distortion is always the height difference between C_{core} and O_{carb}.

	DFT Ref. [1]	DFT (this work)	difference
O_{carb} (1)	2.53	2.49	−0.04
O_{anhyd} (2)	2.71	2.66	−0.05
C_{func} (3)	2.69	2.67	−0.02
C_{core}	2.80	2.85	0.05
molecular distortion	0.27	0.36	0.09
$\Delta(O_{anhyd}/O_{carb})$	0.18	0.16	−0.02
buckling first Ag layer	0.19	0.18	−0.01

APPENDIX F: ERROR BARS FOR THE LEED-IV ANALYSIS OF PCDA/Ag(100)

Table IV supplements Table I with regard to the LEED-IV results, as it lists the results with the respective error bars.

TABLE IV. Adsorption heights and error bars of individual atoms of PTCDA and Ag atoms of the first and second Ag layers for three models optimized by LEED. All numbers are given in angstroms. In all three models, the PTCDA molecule sits on the on-top site [cf. Fig. 2(a)]. The heights of the PTCDA atoms and Ag atoms determined by LEED are referenced with respect to the averaged height of the first Ag layer (Ag surface layer), defined as 0 Å. The second row lists the Pendry R factors (R_P) of the three models. For simplicity, symmetrized error bars are given. The only exception is the central atom Ag number 5 in the down-geometry. Here, only the error in the direction out of the surface is given, as a downward move of the atom within a reasonable range did not lead to the increase of R_P by $RR \times R_{P,min}$ which is required for the error calculation.

		LEED-IV		
atom		Ag5-up	Ag5-down	Ag5-vacancy
	R_P	0.1845	0.1803	0.1705
O_{carb}	1	2.451 ± 0.046	2.536 ± 0.038	2.491 ± 0.042
O_{anhyd}	2	2.674 ± 0.037	2.755 ± 0.034	2.697 ± 0.037
C_{func}	3	2.507 ± 0.074	2.566 ± 0.055	2.550 ± 0.062
C_{core}	4	2.729 ± 0.056	2.815 ± 0.046	2.768 ± 0.053
	5	2.754 ± 0.034	2.806 ± 0.026	2.787 ± 0.030
	6	2.671 ± 0.072	2.727 ± 0.077	2.687 ± 0.064
	7	2.871 ± 0.057	2.957 ± 0.048	2.904 ± 0.045
	8	2.736 ± 0.046	2.820 ± 0.091	2.734 ± 0.102
	9	2.830 ± 0.043	2.860 ± 0.042	2.874 ± 0.041
First Ag layer	1	0.100 ± 0.094	0.140 ± 0.106	0.137 ± 0.092
	2	0.019 ± 0.057	0.058 ± 0.057	0.058 ± 0.048
	3	−0.174 ± 0.080	−0.138 ± 0.076	−0.163 ± 0.073
	4	−0.027 ± 0.083	−0.027 ± 0.083	−0.056 ± 0.073
	5	0.522 ± 0.222	−0.185 + 0.310	(vacant)
	6	−0.006 ± 0.048	0.044 ± 0.046	0.040 ± 0.046
	7	−0.095 ± 0.137	−0.017 ± 0.132	−0.046 ± 0.113
Second Ag layer	1	−2.022 ± 0.084	−1.979 ± 0.074	−1.972 ± 0.079
	2	−1.979 ± 0.100	−1.951 ± 0.079	−1.965 ± 0.103
	3	−1.988 ± 0.129	−1.944 ± 0.114	−1.941 ± 0.129
	4	−1.954 ± 0.050	−1.923 ± 0.053	−1.914 ± 0.049

[1] O. Bauer, G. Mercurio, M. Willenbockel, W. Reckien, C. H. Schmitz, B. Fiedler, S. Soubatch, T. Bredow, F. S. Tautz, and M. Sokolowski, Role of functional groups in surface bonding of planar pi-conjugated molecules, Phys. Rev. B **86**, 235431 (2012).

[2] P. Woodruff, *Surface Structure Methods* (Cambridge University Press, Cambridge, 2016).

[3] W. Moritz and M. Van Hove, *Surface Structure Determination by LEED and x-rays* (Cambridge University Press, 2022).

[4] Z. V. Zheleva, T. Eralp, and G. Held, Complete experimental structure determination of the p(3 × 2)*pg* phase of glycine on Cu{110}, J. Phys. Chem. C **116**, 618 (2012).

[5] R. Lindsay, S. Tomić, A. Wander, M. García-Méndez, and G. Thornton, Low energy electron diffraction study of TiO_2(110)(2 × 1)-$[HCOO]^{-1}$, J. Phys. Chem. C **112**, 14154 (2008).

[6] C. Stellwag, G. Held, and D. Menzel, The geometry of ordered benzene layers on Ru(001), Surf. Sci. **325**, L379 (1995).

[7] T. Sirtl, J. Jelic, J. Meyer, K. Das, W. M. Heckl, W. Moritz, J. Rundgren, M. Schmittel, K. Reuter, and M. Lackinger, Adsorption structure determination of a large polyaromatic trithiolate on Cu(111): Combination of LEED-I(V) and DFT-vdW, Phys. Chem. Chem. Phys. **15**, 11054 (2013).

[8] J. Zegenhagen and A. Kazimirov, eds., *The X-Ray Standing Wave Technique - Principles and Applications, in Series on Synchrotron Radiation Techniques and Applications*, Vol. 7 (World Scientific, NewJersey, 2013).

[9] G. Held, A. Wander, and D. A. King, Variations of LEED intensities with angle of incidence and the influence on spot profiles, Phys. Rev. B **51**, 17856 (1995).

[10] G. Held, Structure determination by low-energy electron diffraction–a roadmap to the future, Surf. Sci. **754**, 122696 (2025).

[11] G. Held, M. P. Bessent, S. Titmuss, and D. A. King, Realistic molecular distortions and strong substrate buckling induced by

the chemisorption of benzene on Ni{111}, J. Chem. Phys. **105**, 11305 (1996).
[12] J. Ikonomov, O. Bauer, and M. Sokolowski, Highly ordered thin films of perylene-3,4,9,10-tetracarboxylic acid dianhydride (PTCDA) on Ag(100), Surf. Sci. **602**, 2061 (2008).
[13] O. Bauer, Surface Bonding of a Functionalized Aromatic Molecule: Adsorption Configurations of PTCDA on Coinage Metal Surfaces, Ph.D. thesis, Rheinische Friedrich-Wilhelms-Universität Bonn, 2014.
[14] S. Weiß, I. Krieger, T. Heepenstrick, S. Soubatch, M. Sokolowski, and F. S. Tautz, Determination of the adsorption geometry of PTCDA on the Cu(100) surface, Phys. Rev. B **96**, 075414 (2017).
[15] H. Li, J. Quinn, Y. S. Li, F. Jona, and P. M. Marcus, Multilayer relaxation of clean Ag(001), Phys. Rev. B **43**, 7305 (1991).
[16] OCI Mircoengineering, Inc., Canada, Technical documentation for back-display LEED-Auger optics models BDL800IR/600IR with mircochannel plates and power supply LPS300-D (2005).
[17] PrismaPlus QMG 220 quadrupole mass spectrometer purchased from Pfeiffer Vacuum GmbH (2011).
[18] J. B. Pendry, *Low Energy Electron Diffraction* (Academic Press, London, 1974).
[19] M. A. Van Hove and S. Y. Tong, *Surface Crystallography by LEED*, Springer series in Solid–State Sciences (Springer, Berlin, 1979).
[20] A. Barbieri and M. A. V. Hove, Barbieri/Van hove phase shift package: A brief user guide (1995), https://pythonhosted.org/phaseshifts/phshift2007.html.
[21] G. Held, W. Braun, H. Steinrück, S. Yamagishi, S. Jenkins, and D. King, Light-atom location in adsorbed benzene by experiment and theory, Phys. Rev. Lett. **87**, 216102 (2001).
[22] W. H. Press, B. P. Flannery, S. A. Teukolsky, and W. T. Vetterling, *Numerical Recipes in C* (Cambridge University Press, Cambridge, 1988).
[23] W. Moritz, B. Wang, M. L. Bocquet, T. Brugger, T. Greber, J. Wintterlin, and S. Guenther, Structure determination of the coincidence phase of graphene on Ru(0001), Phys. Rev. Lett. **104**, 136102 (2010).
[24] J. B. Pendry, Reliability factors for LEED calculations, J. Phys. C: Solid State Phys. **13**, 937 (1980).
[25] See Supplemental Material at http://link.aps.org/supplemental/10.1103/gxh1-b3w4 for the complete set of experimental and calculated IV-curves of PTCDA/Ag(100).
[26] J. W. Furness, A. D. Kaplan, J. Ning, J. P. Perdew, and J. Sun, Accurate and numerically efficient r^2SCAN meta-generalized gradient approximation, J. Phys. Chem. Lett. **11**, 8208 (2020).
[27] R. Kingsbury, A. S. Gupta, C. J. Bartel, J. M. Munro, S. Dwaraknath, M. Horton, and K. A. Persson, Performance comparison of r^2SCAN and SCAN metagga density functionals for solid materials via an automated, high-throughput computational workflow, Phys. Rev. Mater. **6**, 013801 (2022).
[28] G. Kresse and J. Furthmüller, Efficient iterative schemes for ab initio total-energy calculations using a plane-wave basis set, Phys. Rev. B **54**, 11169 (1996).
[29] G. Kresse and J. Furthmüller, Efficiency of ab-initio total energy calculations for metals and semiconductors using a plane-wave basis set, Comput. Mater. Sci. **6**, 15 (1996).
[30] P. E. Blöchl, Projector augmented-wave method, Phys. Rev. B **50**, 17953 (1994).
[31] G. Kresse and D. Joubert, From ultrasoft pseudopotentials to the projector augmented-wave method, Phys. Rev. B **59**, 1758 (1999).
[32] S. Grimme, S. Ehrlich, and L. Goerigk, Effect of the damping function in dispersion corrected density functional theory, J. Comput. Chem. **32**, 1456 (2011).
[33] D. Packwood, J. Kermode, L. Mones, N. Bernstein, J. Woolley, N. Gould, C. Ortner, and G. Csányi, A universal preconditioner for simulating condensed phase materials, J. Phys. Chem. **144**, 164109 (2016).
[34] A. Hjorth Larsen, J. Jørgen Mortensen, J. Blomqvist, I. E. Castelli, R. Christensen, M. Dułak, J. Friis, M. N. Groves, B. Hammer, C. Hargus, E. D. Hermes, P. C. Jennings, P. Bjerre Jensen, J. Kermode, J. R. Kitchin, E. Leonhard Kolsbjerg, J. Kubal, K. Kaasbjerg, S. Lysgaard, J. Bergmann Maronsson, *et al.*, The atomic simulation environment—a python library for working with atoms, J. Phys.: Condens. Matter **29**, 273002 (2017).
[35] J. Enkovaara, C. Rostgaard, J. J. Mortensen, J. Chen, M. Dułak, L. Ferrighi, J. Gavanholt, C. Glinsvad, V. Haikola, and H. A. Hansen, Electronic structure calculations with GPAW: A real-space implementation of the projector augmented-wave method, J. Phys.: Condens. Matter **22**, 253202 (2010).
[36] P. Puschnig, Organic molecule database: A database for molecular orbitals of conjugated organic molecules based on the atomic simulation environment (ASE) and nwchem as the DFT calculator (University of Graz, 2020); https://homepage.uni-graz.at/de/peter.puschnig/research-1/.
[37] H. L. Meyerheim, T. Goege, H. Maltor, M. Sokolowski, E. Umbach, and P. Bäuerle, Bond stretching an distortion in large organic molecules on Ag(111) determined by surface x-ray diffraction, Surface Rev. Lett. **06**, 883 (1999).
[38] We note that for the calculations for the hollow site we utilized different and not fully appropriate vibrational amplitudes. However, this has minor impact on the R factor and none on the conclusions.
[39] H. I. Li, K. Pussi, K. J. Hanna, L. L. Wang, D. D. Johnson, H. P. Cheng, H. Shin, S. Curtarolo, W. Moritz, J. A. Smerdon, R. McGrath, and R. D. Diehl, Surface geometry of C_{60} on Ag(111), Phys. Rev. Lett. **103**, 056101 (2009).
[40] K. Pussi, H. I. Li, H. Shin, L. N. Serkovic Loli, A. K. Shukla, J. Ledieu, V. Fournée, L. L. Wang, S. Y. Su, K. E. Marino, M. V. Snyder, and R. D. Diehl, Elucidating the dynamical equilibrium of C_{60} molecules on Ag(111), Phys. Rev. B **86**, 205406 (2012).
[41] D.-J. Liu, Density functional analysis of key energetics in metal homoepitaxy: Quantum size effects in periodic slab calculations, Phys. Rev. B **81**, 035415 (2010).
[42] J. Ikonomov, P. Bach, R. Merkel, and M. Sokolowski, Surface diffusion constants of large organic molecules determined from their residence times under a scanning tunneling microscope tip, Phys. Rev. B **81**, 161412(R) (2010).
[43] J. Ikonomov, C. H. Schmitz, and M. Sokolowski, Diffusion-limited island decay of PTCDA on Ag(100): Determination of the intermolecular interaction, Phys. Rev. B **81**, 195428 (2010).
[44] X. Yang, I. Krieger, D. Lüftner, S. Weiss, T. Heepenstrick, M. Hollerer, P. Hurdax, G. Koller, M. Sokolowski, P. Puschnig, M. G. Ramsey, F. S. Tautz, and S. Soubatch, On the decou-

pling of molecules at metal surfaces, Chem. Commun. **54**, 9039 (2018).

[45] C. Brülke, T. Heepenstrick, I. Krieger, B. Wolff, X. Yang, A. Shamsaddinlou, S. Weiss, F. C. Bocquet, F. S. Tautz, S. Soubatch, and M. Sokolowski, Quantitative analysis of the electronic decoupling of an organic semiconductor molecule at a metal interface by a monolayer of hexagonal boron nitride, Phys. Rev. B **99**, 121404(R) (2019).

[46] M. Hochheim, A. Paulheim, M. Sokolowski, and T. Bredow, Analysis of the vibronic spectra of perylene-3,4,9,10-tetracarboxylic dianhydride adsorbed on NaCl and KCl, J. Phys. Chem. C **120**, 24240 (2016).

[47] L. Kilian, A. Hauschild, R. Temirov, S. Soubatch, A. Schoell, A. Bendounan, F. Reinert, T. L. Lee, F. S. Tautz, M. Sokolowski, and E. Umbach, Role of intermolecular interactions on the electronic and geometric structure of a large π-conjugated molecule adsorbed on a metal surface, Phys. Rev. Lett. **100**, 136103 (2008).

[48] I. Krieger, M. Sokolowski, A. Haags, T. Bredow, C. Kumpf, F. S. Tautz, and G. Held, Structure analysis of PTCDA/Ag(100) by low energy electron diffraction and density functional theory (2025), https://doi.org/10.26165/JUELICH-DATA/V2XQ53.

[49] J. Wang, Low Energy Electron Diffraction Studies of Transition Metal Oxide Surfaces and Films, Ph.D. thesis, Martin-Luther-Universität Halle-Wittenberg, 2005.

[50] P. Bohnen, T. Rodach, and K. Ho, *The Structure of Surfaces III*, edited by S. Tong and M. V. Hove (Springer Verlag, New York, 1991).

[51] I. N. Levine, *Physical Chemistry* (McGraw-Hill, New York, 2001).